Petrography and Geochemistry of the Jajarm Karst Bauxite Ore Deposit, NE Iran: Implications for Source Rock Material and Ore Genesis

DARIUSH ESMAEILY, HOSEIN RAHIMPOUR-BONAB,
AMIR ESNA-ASHARI & ALI KANANIAN

Department of Geology, College of Science, University of Tehran, 14155–6455 Tehran, Iran

(E-mail: esmaili@khayam.ut.ac.ir)

Abstract: The Jajarm bauxite deposit, northeast Iran, is the largest such deposit in Iran. The deposit is sandwiched between the Triassic Elika formation and the Jurassic Shemshak formation, housed within karstic features developed within the former unit. The deposit generally shows an internal layering defined by the following four distinct horizons (from bottom to top): (a) a lower argillaceous horizon, approximately 50–80 cm thick, is mainly composed of clay minerals that directly overlies the carbonate footwall (Elika formation); (b) a bauxitic clay layer approximately 2–3 m thick that consists mainly of hematite, kaolinite, anatase, and diaspore; (c) a red bauxite layer (the main high-grade ore), about 5 m thick and composed of diaspore, kaolinite, anatase, and hematite; and (d) an upper kaolinitic layer that is 20–50 cm thick, composed mainly of kaolinite, and overlain by the Shemshak formation. Detailed petrographic studies reveal diagenetic alteration of the bauxitic protolith. The main observed bauxite textures are microgranular, oolitic, pisolitic, fluidal-collomorphic, and microclastic. Microgranular and microclastic textures associated with the residual fractured and corroded quartz grains, as well as feldspar grains are almost completely replaced by platy diaspore. Geochemical analyses of the red bauxite reveal enrichment of less mobile elements (Nb, Th, Zr, Mo, Ga, and Cr) and depletion of mobile elements (Rb, K, Na, Sr, La, Mg, and Pb); the opposite result is obtained for the bauxitic clay. Chondrite-normalized REE (Rare Earth Element) patterns for the upper kaolinite layer are similar to those for the underlying red bauxite, and the patterns obtained for the lower argillaceous layer are similar to those for the overlying argillaceous bauxite horizon. Ce shows a positive anomaly in the red bauxite and a negative anomaly in the bauxitic clay. The correlation coefficients calculated between REE and other elements demonstrate that the likely REE-bearing minerals are oxides of Ti and Nb, clay minerals, and zircon. In contrast to the present diasporic mineralogical composition of the Jajarm bauxite, the geochemical and mineralogical data indicate an original gibbsitic composition. Finally, the observed mineralogical and textural evidence, combined with the evidence provided by variation diagrams and REE patterns, indicates a mixed origin for the Jajarm bauxite from both basic igneous and sedimentary rocks. In fact, bauxitization was initiated on basic source rocks and continued during reworking and replacement within the karstic features.

Key Words: Iran, karst bauxite, geochemistry, diaspore, ore deposit

Jajarm (KD İran) Karst Boksit Cevher Yatağının Petrografisi ve Jeokimyası: Kaynak Kaya Materyali ve Cevher Kökeni İçin Göstergeler

Özet: İran'ın kuzeydoğusunda bulunan Jajarm boksit yatağı İran'daki en büyük yataktır. Yatak, Trias yaşlı Elika formasyonu ve Jura yaşlı Shemshak formasyonu arasında yüzeylemektedir. Yatak genel olarak dört farklı düzeyi (alttan üste doğru) takiben tanımlanan bir iç katman yapısı göstermektedir: (a) direkt olarak karbonat (Elika Formasyonu) tabanını üzerleyen, başlıca kil minerallerinden yapılı yaklaşık olarak 50–80 cm kalınlığındaki alt arjilikli seviye, (b) başlıca hematit, kaolinit, anatas ve diyaspor minerallerinden meydana gelen ve yaklaşık olarak 2–3 m kalınlığındaki bir boksitik kil seviyesi, (c) diyaspor, kaolinit, anatas ve hematit minerallerinden yapılı olan ve 5 m kalınlığındaki kırmızı boksit seviyesi (yüksek tenörlü ana cevher), (d) başlıca kaolinitten yapılı olan 20–50 cm kalınlığındaki üst kaolinit seviyesi ve bu seviye Shemshak formasyonu tarafından üzerlenmektedir. Detaylı petrografik çalışmalar, boksitik

protolitin diyajenetik alterasyonunu göstermektedir. Çalışılmış örneklerde gözlenen boksit dokuları mikrogranüler, oolitik, pizolitik, kolloform ve mikroklastiktir. Feldspat tanelerinin yanısıra, kırılmış ve aşınmış kalıntı kuvars taneleri ile ilişkili mikrogranüler ve mikroklastik dokular, hemen hemen komple levhasal diyaspor tarafından yeri alınmıştır. Kırmızı boksitin jeokimyasal analizleri mobil elementlerin (Rb, K, Na, Sr, La, Mg, and Pb) tüketildiğini, daha az mobil elementlerin (Nb, Th, Zr, Mo, Ga, and Cr) ise zenginleştiğine işaret etmektedir. Zıt bir sonuç, boksitik kil için gözlenmektedir. Üst kaolinit seviyesi için kondrite göre normalize edilmiş NTE (Nadir Toprak Elementleri) örgüleri altlayan kırmızı boksitlerinkilere benzerdir, ve alt arjilikli seviye için gözlenen örgüler, üzerleyen arjilikli boksit seviyesindekine benzerdir. Ce, boksitik kilde bir negatif anomali ve kırmızı boksitte bir pozitif anomali gösterir. NTE ve diğer elementler arasında hesaplanmış olan korelasyon katsayıları, NTE-içeren minerallerin Ti ve Nb, kil mineralleri, ve zirkonun oksitleri olduğunu ortaya koymaktadır. Jajarm boksitlerinin var olan diyasporik mineralojik bileşiminin aksine, jeokimyasal ve mineralojik veriler, orijinal jipsitik bir bileşime işaret eder. Sonuç olarak, değişim diyagramları ve NTE örgüleri ile sağlanan kanıt ile gözlenen mineralojik ve dokusal ilişkiler, Jajarm boksiti için hem bazik hem de sedimanter kayaçlardan oluşan karışmış bir kökeni işaret etmektedir. Aslında, boksitleşme bazik köken kayaçlar üzerinde başlamış ve karstik özellikler içerisinde yerleşim ve yeniden işlenmesi süresince devam etmiştir.

Anahtar Sözcükler: İran, karst boksit, jeokimya, diyaspor, cevher yatağı

Introduction

Lateritic bauxite deposits developed in tropical regions principally consist of hydrated aluminium minerals such as gibbsite $Al(OH)_3$, boehmite $AlO.OH$, and diaspore $AlO.OH$. These minerals contain variable amounts of iron, silicon and titanium as atomic substitution for Al, and other elements in minor and/or trace amounts (e.g., Th, P, Y, Ga, Ge and V), either incorporated in the mineral lattice or adsorbed onto its surface (Shaffer 1975; Bárdossy & Aleva 1990; Mordberg 1999; Öztürk *et al.* 2002). Diaspore is the most stable bauxite mineral at the temperature and pressure conditions of the earth surface, especially in dry areas, whereas gibbsite, in contrast to diaspore and boehmite, is more stable in humid climates but it still dissolves in weathering environments (Furian 1994; Dedecker & Stoops 1999) and its dissolution is pH dependent (Nahon 1991, p. 186; Velde 1992, p. 107).

Bauxite deposits are commonly classified as one of three genetic types according to mineralogy, chemistry, and host-rock lithology (Bárdossy & Aleva 1990). Of all the known bauxite deposits, about 88% are lateritic type, 11.5% are karst type, and the remaining 0.5% are Tikhvin type (Bárdossy 1982; Bárdossy & Aleva op. cit.). The specific conditions that give rise to different paths of bauxite formation have been documented previously (e.g., Bárdossy & Aleva op. cit.). Lateritic-type deposits form upon aluminosilicate rocks via *in-situ* lateritization. In such cases, the most important factors in determining the extent and grade of bauxite formation are the parent rock composition, climate, topography, drainage, groundwater chemistry and movement, location of the water table, microbial activity, and the duration of weathering processes (Grubb 1963; Bárdossy & Aleva 1990; Price *et al.* 1997). Karst-type deposits occur within depressions upon karstified or eroded surfaces that formed upon carbonate rocks. Such deposits originate from a variety of different materials, depending upon the source area (Bárdossy 1982). Finally, Tikhvin-type deposits are transported or allochthonous deposits that overlie alumosilicate rocks and that originate from pre-existing residual laterite profiles (Bárdossy 1982, p. 21; Bárdossy & Aleva 1990, p. 63).

In recent decades, various studies have investigated the occurrence within bauxite deposits of most of the known chemical elements (e.g., Bronevoi *et al.* 1985; Bárdossy & Aleva 1990; Maksimović & Pantó 1991; MacLean *et al.* 1997; Eliopoulos & Economou-Eliopoulos 2000; Mutakyahwa *et al.* 2003). In profiles of particular deposits or bauxitic districts, most of these earlier studies describe details of the distribution and behaviour of different elements, as well as the process of bauxite genesis.

Bauxites of Upper Triassic to Upper Cretaceous age are widespread throughout Iran, especially in Central Iran and the Alborz Mountain Range (Figure 1a). The layered Jajarm bauxite ore deposit, located 18 km from the town of Jajarm (Khorasan province,
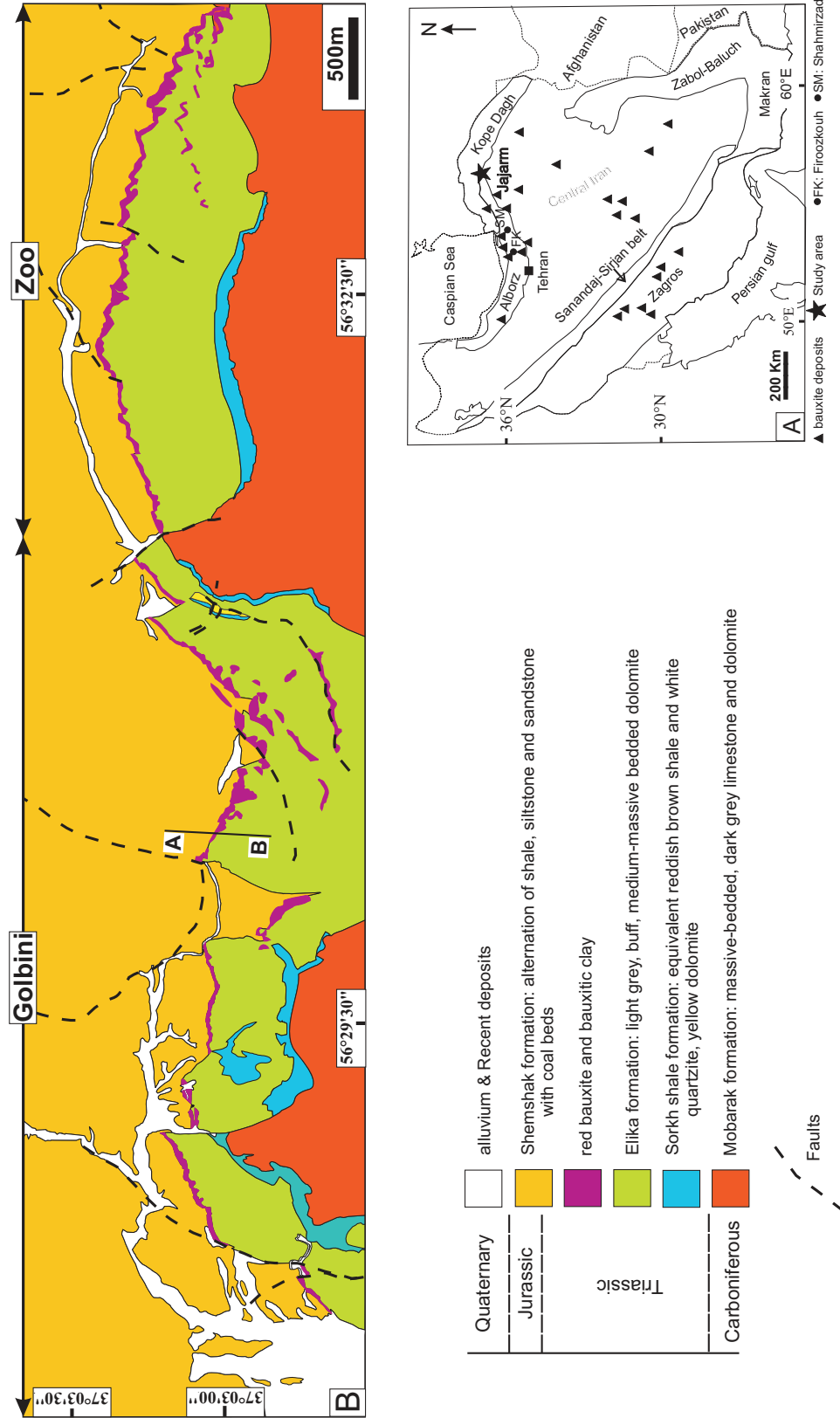
Figure 1. (**A**) Location of the bauxite deposits on the geographical sketch map of Iran (Berberian & King 1981): the Jajarm bauxite marked by star; (**B**) simplified geological map of the Jajarm bauxite deposit and its surrounding units.

Northeast Iran) and 620 km from Tehran (Figure 1), is more than 8 km long and 20 m thick, making it the largest bauxite deposit in Iran. The few detailed geological data for this area mainly comprise exploration, extraction and reconnaissance reports.

The first exploration for bauxite in Jajarm began in 1970 when the Geological Survey of Iran (GSI) carried out extensive exploration work in this part of the country; the exploration for bauxite began in the area in 1999. A feasibility study on the Jajarm bauxite ore deposit was carried out in 1999 by the Tectono-export Company and an alumina production plant was constructed near the mine site in 2001. The bauxite resource at Jajarm is estimated to contain more than 19 Mt ore with an Al_2O_3/SiO_2 ratio of 43/14. The bauxite ore is currently mined from an open pit and processed in the alumina production plant.

The present paper aims to provide geological, petrographic and geochemical data on the Jajarm bauxite deposit and aspects of its origin are discussed.

Geological Setting

The Jajarm bauxite deposit is situated in the eastern part of the Alborz structural zone (Figure 1). Lower Devonian sandstone, evaporites, and limestone of the Padha formation are the oldest rocks in the area. The Upper Devonian Khosh Yeylagh formation consists of fossiliferous limestone, dolomite, shale, and sandstone, and is overlain by Lower Carboniferous shale and carbonate of the Mobarak formation (Figure 1). There are no Middle and Upper Carboniferous sediments in the area. Brown indurated claystones and siltstones with small iron concretions overlie the Mobarak formation. In the sense of Brönnimann *et al.* (1973) this layer is equivalent of Sorkh Shale formation named by Stöcklin *et al.* (1965) in eastern Central Iran (Tabas area and Shotori Range). Because of its red colour and rather argillaceous composition it was named the Sorkh Shale formation (Sorkh= red) and it is in turn overlain by the Lower Triassic Elika carbonates.

The Elika formation, that hosts the Jajarm karst bauxite, is approximately 215 m thick and is divided into two parts: the lower part consists of thinly bedded dolomite and dolomitic limestone, with lesser marl and yellowish shale (approximately one-third of the total thickness of the formation), while the upper part consists of thick light-brown to dark yellow and grey dolomite layers that define the highlands and mountains of the area.
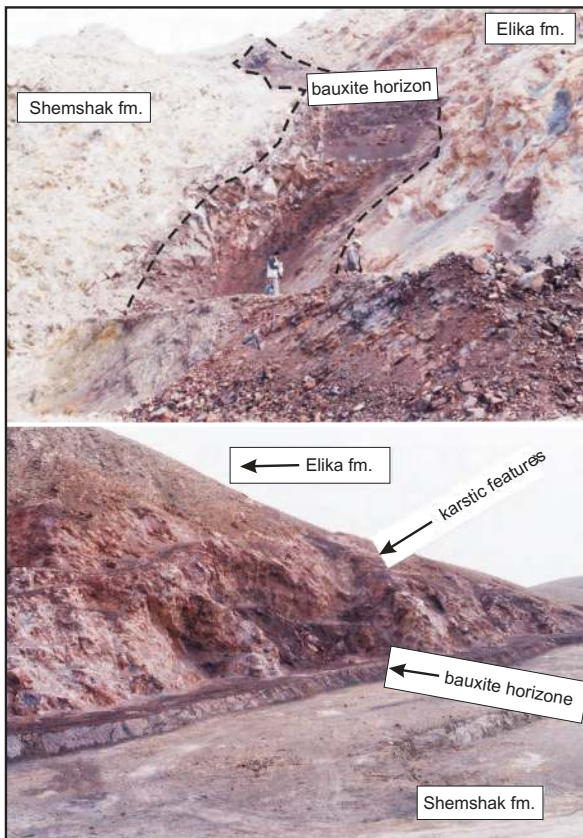
In many areas throughout the Alborz Mountain Range, including some locations close to the study area, the Elika formation is overlain by dark crystalline basic volcanic rocks. Palaeontological studies in the eastern part of the Alborz zone confirm the absence of Upper Triassic marine sediments in this area (Stampfli *et al.* 1976; Seyed-Emami *et al.* 2005) (Figure 2). The karst features that host the Jajarm bauxite deposit formed within thick dolomites of the upper Elika formation. Development of the karst topography in the Elika formation occurred in its upper dolomitic and resistant section (Figures 2 & 3). Alternating shale and sandstone of the coal-rich Jurassic Shemshak formation (202 m thick) disconformably overlies the bauxite horizon. Thus, the karst bauxite formed in the upper parts of the Elika formation and is sandwiched between the latter unit and the Shemshak formation.

During the Triassic and Jurassic, closure of the Palaeotethys Ocean initiated subduction of the oceanic lithosphere of the Neotethys Ocean beneath the Eurasian Plate (Berberian & Berberian 1981; Berberian & King 1981; Hooper *et al.* 1994, among others). Movement of the Afro-Arabian plate toward
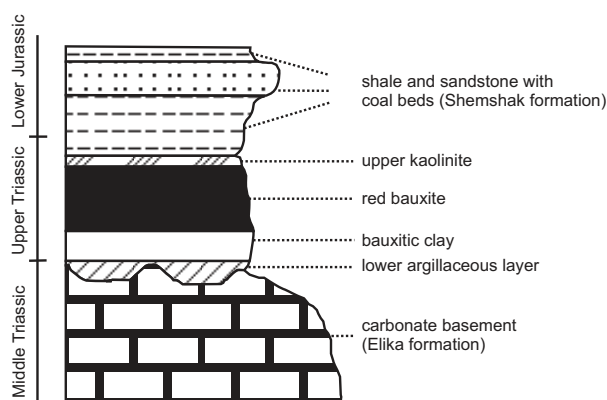
Figure 2. Stratigraphic column of the studied section in the Jajarm area. Irregular right boundary shows the difference of hardness degree for each layer.

Figure 3. Outcrops of the Jajarm bauxite with its footwall (Elika formation) and hanging wall (Shemshak formation). As seen, karstic features show irregular morphology and hosted bauxite deposit.

subaerial exposure of Triassic dolomites (Elika formation) in a tropical climate, resulting in karstification.

This karstified carbonate hosted the Jajarm bauxite and was buried by several thousand metres of younger sediments, beginning with the Jurassic Shemshak formation and other younger units.

Mine Geology

The Jajarm bauxite deposit is located in an area folded into an E–W-trending anticline, cut by several reverse faults, so that its northern extension is overthrust on to the southern part. This overthrusting has hidden the bauxite deposit beneath Quaternary units. As a result, the bauxite deposit is only exposed on the northern flank of the anticline, along a length of about 8 km. Exposure of the ore body is discontinuous along its length, with the deposit occurring as isolated blocks that for mining purposes are subdivided into eight blocks in the Golbini area and four in the Zoo area (Figure 1). The variation of $Al_2O_3:SiO_2$ ratios from 0.87 to 7.52 throughout the deposit means that ore grades are locally heterogeneous.

A complete profile through the Jajarm bauxite deposit reveals an internal stratigraphy (layering) characterized by the following four distinct horizons (from bottom to top): (a) a lower argillaceous layer, (b) bauxitic clay, (c) red bauxite, and (d) an upper kaolinitic layer (Figure 2). The lower argillaceous horizon, about 50–80 cm thick, which is mineralogically heterogeneous, directly overlies the carbonate footwall (Elika formation) of the deposit and is mainly composed of clay minerals (in particular kaolinite and illite) and anatase, with lesser diaspore, hematite, pyrite, and goethite. The colour of this layer changes from grey (G 5/5 according to Munsel chart) at its base (close to the carbonate footwall) to pinkish and red (R 4/4) at its top (close to the bauxitic clay layer).

The bauxitic clay layer is about 2–3 m thick, dominated by clay minerals (mainly kaolinite and illite), hematite, anatase, and diaspore, with rare rutile and quartz, and sharply overlies the lower argillaceous layer. Layering is locally visible, but the clay layer is not economically viable in terms of

Eurasia meant that central Iran and the Alborz structural zone were located in the tropics at this time (Berberian 1983). The dominance of shallow water carbonate environments is one of the main features of the Tethys Basin, resulting in the formation of thick carbonate units, some hosting bauxite deposits (e.g., the Elika formation). During the late Permian, these carbonate shelves were distributed around the entire Gondwanaland margin and parts of the Tethys (Marcoux 1993). Following a Lower Triassic transgression, the Elika formation was deposited in the Alborz zone and the Jajarm area. A progressive sea-level fall during the Middle Triassic caused development of sabkha environments in the area (Stampfli *et al.* 1976). Finally, during the late Middle Triassic or early Upper Triassic, a fall in sea level led to an epeirogenetic phase and the

alumina production. The clay is friable, and its colour varies from bright to dark red (R 4/3 to R 5/8).

The red bauxite, which is approximately 5 m thick, is the main high-grade ore extracted for the production of alumina. This horizon is physically harder than the others, and is mainly red in colour (R 5/8), although locally green. The boundary between this horizon and the bauxitic clay is gradual. Minerals identified in this horizon include diaspore, kaolinite, anatase, berthierine, and hematite, along with lesser illite, quartz, rutile, and boehmite. Berthierine, which forms under reducing conditions (e.g., Iijima & Matsumoto 1982; Mordberg 1999), gives rise to the locally green colour (G 5/4) of the horizon.

The upper kaolinite layer is grey (G 5/6), 20–50 cm thick, mainly composed of kaolinite associated with other minerals such as anatase and hematite and overlain by the Shemshak formation. The lower boundary of this layer is very irregular but sharp.

Sampling and Analytical Methods

A total of about 500 rock samples were collected from the four layers described above. Samples were collected from different chips and along bottom to top of the profiles in different sections. Two hundred thin sections and polished thin sections were studied by optical microscopy. Thirty-two representative samples were then selected for whole-rock chemical and X-ray diffraction (XRD) analysis. 2–3 kg samples were crushed and powdered. Major and trace element concentrations were determined by inductively coupled plasma atomic emission spectrometry (ICP-AES) and inductively coupled plasma-mass spectrometry (ICP-MS) at Activation Laboratories, Ontario, Canada. The analytical procedure is described in Cotten et al. (1995). Relative standard deviations were ≤ ±2% for major elements and ≤ ±5% for trace elements. The results of the analyses are provided in Table 1.

Mineralogical analyses were carried out using a Siemens D4 automatic diffractometer. Samples were scanned with a step size of 0.020 and a step time of 1 s, using Cu Kα radiation from a Cu anode X-ray (1.5406 Å).

Mineralogy and Texture

Detailed textural and mineralogical analysis based on the optical microscopy and XRD data was carried out. It showed that diaspore, the main Al-bearing hydroxide in the Jajarm bauxite, generally appears as a replacement and void-filling cement. In the latter case, it occurs as coarse-grained crystals that locally show features of reworking (Figure 4a). Some intraclast grains consist of various fragments that are well-cemented by diaspore. The most important silicate minerals that accompany diaspore are kaolinite (as reactive silica) and minor quartz (as non-reactive silica). Hematite is the most important Fe-bearing mineral, producing the red colour of the deposit. Some samples contain minor berthierine and rare boehmite. Berthierine is an iron-rich, aluminous, l: l-type layer silicate belonging to the serpentine group (Brindley 1981). XRD data showed berthierine to be a minor constituent of some bauxite samples along with other rock forming minerals.

In some samples reworked, fractured and corroded quartz grains are embedded in a matrix of diaspore, iron oxides, or kaolinite. Many samples that contain older fragments of well-rounded diaspore intraclasts and aggregates are now cemented by a matrix of fine-grained diaspore and iron oxyhydroxides (Figure 4b). This texture suggests the transportation and re-deposition of bauxite, at least locally. The heterogeneous distribution of iron oxyhydroxides is indicated by the variable colouring of many samples, ranging from intense red to light brown.

The matrix-forming minerals are generally 1–20 mm in size, although some diasporic minerals are 100–200 mm (Figure 4a, b). The wide ranges in crystal size may reflect the old age of the deposit and the influence of such processes as alteration, recrystallization and diagenesis (Figure 4c). The effects of early and burial diagenesis, accompanied by tectonic stresses, have led to recrystallization and the growth of large crystals. The grain sizes of detrital particles such as intraclasts and diagenetic particles such as ooids and pisoids vary from several microns to several millimetres (Figure 4a, c). Presumably, during bauxitic material formation in the source area and in the karstic depressions, the

Table 1. Major and trace element contents of the Jajarm bauxite.

	Bauxitic Clay											range		average	Lower Argillaceous Layer					range		average
sample	A036	A006	A010	A013	A015	A017	A019	A022	A026	A029	A031	Min	Max		A001	A005	A009	A021	A025	Min	Max	
wt%																						
SiO$_2$	29.4	30.5	26.1	17.8	27.7	28.3	25.0	24.4	31.4	24.4	35.3	17.8	35.3	27.3	8.5	38.4	28.8	44.5	37.4	8.5	44.5	30.8
Al$_2$O$_3$	36.1	29.7	26.5	33.0	38.0	33.2	37.6	42.5	38.6	29.3	29.6	26.5	42.5	34.0	57.7	29.0	47.0	34.6	30.1	29.0	57.7	38.7
Fe$_2$O$_3$	16.7	23.0	32.2	34.2	16.5	21.5	20.3	14.6	9.9	31.5	17.8	9.9	34.2	21.6	7.7	12.3	2.6	0.6	15.3	0.6	21.6	10.0
MnO	0.05	0.02	0.02	0.03	0.01	0.02	0.01	0.01	0.04	0.01	0.02	0.01	0.05	0.02	0.00	0.00	0.00	0.00	0.00	0.00	0.02	0.00
MgO	0.60	0.17	0.34	0.09	0.10	0.15	0.13	0.26	0.26	0.11	0.29	0.09	0.60	0.23	0.13	0.50	0.32	0.48	0.36	0.13	0.50	0.34
CaO	0.13	0.20	0.48	0.05	0.22	0.12	0.10	0.11	0.52	0.14	0.14	0.05	0.52	0.20	0.03	0.22	0.15	0.20	0.21	0.03	0.22	0.17
Na$_2$O	0.06	0.03	0.04	0.03	0.03	0.06	0.03	0.08	0.08	0.03	0.07	0.03	0.08	0.05	nd	0.11	0.07	0.17	0.12	0.05	0.17	0.10
K$_2$O	0.58	0.39	0.22	0.61	0.19	0.49	0.46	1.97	0.89	0.42	1.42	0.19	1.97	0.69	1.38	7.70	4.36	7.59	2.80	0.69	7.70	4.09
TiO$_2$	2.8	3.5	2.6	3.7	3.8	4.2	3.7	3.9	4.5	3.1	3.4	2.6	4.5	3.6	5.9	3.0	4.9	3.5	3.1	3.0	5.9	4.0
P$_2$O$_5$	0.10	0.19	0.08	0.16	0.12	0.14	0.14	0.13	0.08	0.07	0.17	0.07	0.19	0.13	0.19	0.22	0.12	0.16	0.14	0.12	0.22	0.16
LOI	12.3	11.0	10.2	9.2	12.3	11.1	11.4	10.7	12.6	9.7	10.7	9.2	12.6	11.0	17.3	7.1	10.4	7.3	10.2	7.1	17.3	10.5
total	98.9	98.7	98.7	98.9	99.0	99.2	98.8	98.7	98.9	98.8	98.9				98.8	98.6	98.7	99.1	99.8			
ppm																						
Ba	35	102	40	57	56	66	63	148	32	32	173	32	173	73	14	177	46	146	1041	14	1041	250
Sr	272	946	311	542	412	453	672	629	383	305	780	272	946	519	1209	1158	523	759	509	509	1209	779
Y	21	83	89	42	22	108	57	60	22	83	65	21	108	59	67	87	41	77	95	59	95	76
Sc	42	40	42	57	39	50	45	43	38	35	31	31	57	42	40	32	41	31	35	31	42	37
Zr	417	511	417	474	532	570	572	546	607	488	476	417	607	510	838	430	712	530	450	430	838	578
Be	3	6	5	5	3	6	5	6	2	5	6	2	6	4	5	2	4	4	5	2	5	4
V	350	411	574	516	485	522	453	396	497	428	423	350	574	460	736	442	496	492	453	442	736	513
Cr	155	108	141	96	129	156	139	149	176	202	132	96	202	144	288	112	215	152	119	112	288	172
Co	118	13	110	13	8	22	16	23	24	19	34	8	118	36	35	7	7	20	16	7	36	20
Ni	178	112	147	78	69	118	119	154	30	114	134	30	178	114	121	61	92	118	109	61	121	102
Cu	nd	nd	nd	nd	nd	42	nd	nd	33	nd	38	33	42	37	26	63	25	46	nd	25	63	39
Zn	63	39	78	50	39	124	48	66	36	39	39	36	124	64	nd	39	nd	39	52	39	64	48
Ga	58	nd	29	nd	35	42	nd	45	44	42	31	29	58	42	68	33	56	31	41	31	68	45
Ge	2	3	4	3	2	3	3	3	3	3	2	2	4	3	3	1	5	2	3	1	5	3
As	27	12	29	20	16	39	14	17	23	40	21	12	40	23	24	16	82	18	105	16	105	45
Rb	11	9	7	14	4	11	10	43	17	10	34	4	43	15	25	141	78	138	67	15	141	77
Nb	104	102	93	117	130	140	126	118	132	113	99	93	140	116	148	95	158	117	96	95	158	122
Mo	nd	3	8	3	3	4	4	3	2	5	3	2	8	4	nd	6	10	2	4	2	10	5
Ag	nd	1.2	nd	nd	0.5	nd	nd	nd	0.6	nd	0.9	0.5	1.2	0.8	2.0	1.1	0.5	0.6	nd	0.5	2.0	1.0
In	nd	nd	nd	nd	nd	nd	nd	nd	nd	nd	nd				nd	nd	nd	nd	nd			
Sn	5	5	5	6	6	6	6	6	2	5	6	5	6	6	4	5	7	6	7	4	7	6
Sb	3	6	8	8	4	8	5	5	2	9	4	2	9	6	3	2	2	1	5	1	6	3
Cs	nd	1.0	1.4	0.7	nd	0.8	0.7	2.6	0.9	0.9	2.9	0.7	2.9	1.3	0.8	3.8	2.3	3.8	3.9	0.8	3.9	2.6
La	225	183	84	191	234	268	106	129	25	95	107	25	268	150	88	201	234	146	218	88	234	173
Ce	1080	180	152	443	332	353	215	192	279	215	189	152	1080	330	205	240	198	254	243	198	330	245
Pr	44	34	24	36	26	58	27	40	7	26	30	7	58	32	30	71	66	46	68	30	71	52
Nd	173	97	141	95	56	221	112	154	26	109	139	26	221	120	136	258	159	180	195	120	258	175
Sm	35	17	46	16	7	45	23	29	5	25	29	5	46	25	31	42	18	29	28	18	42	29
Eu	8.6	4.6	14.5	4.0	1.7	11.9	5.4	7.4	1.3	6.9	7.3	1.3	14.5	6.7	7.1	9.3	3.5	5.8	6.3	3.5	9.3	6.5
Gd	23	16	47	11	5	40	16	24	4	23	23	4	47	21	18	23	14	19	23	14	23	20
Tb	3.0	2.4	6.3	1.8	0.7	5.3	2.6	4.0	0.7	3.9	3.1	0.7	6.3	3.1	2.7	2.9	2.3	2.9	3.2	2.3	3.2	2.8
Dy	13	13	27	11	5	23	14	20	3	19	14	3	27	15	14	15	15	17	19	14	19	16
Ho	2.2	2.6	4.4	2.3	1.0	3.8	2.6	3.5	0.7	3.6	2.5	0.7	4.4	2.6	2.6	3.0	3.6	3.6	3.8	2.6	3.8	3.2
Er	7	8	10	7	3	11	8	10	2	11	7	2	11	8	8	10	13	12	13	8	13	10
Tm	1.0	1.1	1.3	1.0	0.5	1.5	1.3	1.6	nd	1.6	1.1	0.5	1.6	1.2	1.2	1.5	2.3	1.8	2.1	1.2	2.3	1.7
Yb	7	7	8	7	3	9	8	10	2	10	7	2	10	7	9	11	16	11	13	7	16	11
Lu	1	1	1	1	nd	1	1	2	nd	2	1	1	2	1	1	2	2	2	2	1	2	2
Hf	11	11	11	11	13	15	14	14	15	13	12	11	15	13	20	11	18	13	11	11	20	14
Ta	7	6	6	8	8	9	8	8	9	7	7	6	9	7	6	6	10	7	6	6	10	7
w	18	10	18	29	14	15	15	28	11	20	16	11	29	18	16	11	20	11	11	11	20	14
Tl	0.2	0.2	1.8	0.3	0.2	0.2	0.1	0.4	0.2	0.2	0.4	0.1	1.8	0.4	0.5	1.3	0.7	1.0	0.6	0.4	1.3	0.8
Pb	13	26	33	33	45	48	23	26	11	35	42	11	48	30	58	63	31	29	33	29	63	41
Bi	10	7	5	4	2	2	6	10	4	8	9	2	10	7	1	3	8	5	14	1	14	6
Th	20	20	19	20	23	25	22	26	25	21	21	19	26	22	31	21	31	22	22	21	31	25
U	10	7	12	40	11	15	9	11	14	15	10	7	40	14	25	25	20	10	12	10	25	18

Table 1. Continued.

sample	Red Bauxite											range		average	Upper Kaolinite					range		average
	A003	A007	A011	A014	A016	A018	A020	A023	A027	A030	A032	Min	Max		A004	A008	A012	A024	A028	Min	Max	
wt%																						
SiO_2	11.2	9.8	29.0	6.9	4.3	6.3	28.2	17.5	19.3	41.8	5.8	4.3	41.8	16.4	39.3	36.4	31.9	34.1	35.7	31.9	39.3	35.5
Al_2O_3	49.2	42.4	33.7	56.5	47.1	49.6	39.8	37.4	35.9	36.4	43.5	33.7	56.5	42.9	33.2	31.2	31.8	29.5	30.8	29.5	33.2	31.3
Fe_2O_3	16.3	28.3	20.2	14.0	27.2	22.2	12.9	26.4	26.6	2.8	31.0	2.8	31.0	20.7	6.9	13.3	10.1	18.1	13.9	6.9	18.1	12.5
MnO	0.11	0.04	0.00	0.01	0.27	0.12	0.08	0.04	0.02	0.01	0.31	0.00	0.31	0.09	0.00	0.31	0.00	0.23	0.22	0.00	0.31	0.15
MgO	0.45	0.53	0.10	0.27	0.14	0.27	0.18	0.86	0.98	0.16	0.36	0.10	0.98	0.39	0.14	0.14	0.24	0.12	0.15	0.12	0.24	0.16
CaO	1.77	0.16	0.08	0.04	2.29	0.88	0.09	0.12	0.16	0.10	0.37	0.04	2.29	0.55	0.76	0.35	0.24	1.03	0.96	0.24	1.03	0.67
Na_2O	0.04	0.05	0.06	0.05	0.02	0.05	0.05	0.04	0.04	0.07	0.02	0.02	0.07	0.04	0.04	0.05	0.17	0.05	0.06	0.04	0.17	0.07
K_2O	1.34	0.26	0.63	0.17	0.77	0.43	0.26	0.46	0.62	0.87	0.24	0.17	1.34	0.55	0.52	1.01	1.93	0.22	0.35	0.22	1.93	0.81
TiO_2	5.5	5.5	3.7	7.1	5.3	6.4	4.3	5.8	4.5	4.2	5.3	3.7	7.1	5.2	3.5	4.0	3.6	4.0	3.7	3.5	4.0	3.8
P_2O_5	0.05	0.10	0.03	0.08	0.15	0.14	0.02	0.10	0.08	0.01	0.06	0.01	0.15	0.07	0.04	0.02	0.05	0.08	0.03	0.02	0.08	0.04
LOI	13.0	12.0	11.4	13.8	11.7	12.2	13.0	10.6	10.8	12.8	11.7	10.6	13.8	12.1	14.2	12.1	18.7	12.4	12.8	12.1	18.7	14.0
total	99.0	99.2	98.7	98.9	99.2	98.6	98.9	99.3	98.8	99.1	98.6				98.6	98.9	98.7	99.8	98.7			
ppm																						
Ba	21	2256	9	333	57	110	30	134	86	22	2666	9	2666	520	925	184	62	108	41	41	925	264
Sr	329	505	86	358	437	1054	87	229	329	71	332	71	1054	347	181	68	237	165	103	68	237	151
Y	53	41	16	49	19	54	35	56	28	17	23	16	56	36	14	30	24	19	23	14	30	22
Sc	34	58	38	46	31	50	45	46	38	30	48	30	58	42	26	39	39	31	35	26	39	34
Zr	809	792	527	1020	771	894	643	749	620	609	691	527	1020	739	520	534	608	518	507	507	608	537
Be	3	3	2	5	2	3	2	2	2	2	1	1	5	2	1	3	1	2	3	1	3	2
V	501	581	607	705	526	692	549	551	482	448	549	448	705	563	408	403	482	412	402	402	482	421
Cr	256	240	198	287	256	280	210	193	189	182	232	182	287	229	169	174	199	151	151	151	199	169
Co	53	47	13	55	32	26	109	86	52	15	25	13	109	47	4	490	3	73	82	3	490	130
Ni	71	87	42	125	nd	35	81	94	69	nd	nd	35	125	76	25	101	24	37	44	24	101	46
Cu	nd	nd	75	23	nd	10	58	nd	nd	243	nd	10	243	82	20	66	201	172	264	20	264	145
Zn	82	62	41	115	44	114	41	57	60	33	33	33	115	71	nd	102	42	46	nd	46	102	74
Ga	61	62	41	68	52	68	41	49	49	28	51	28	68	52	34	33	42	29	37	29	42	35
Ge	3	4	2	3	3	4	2	3	3	1	2	1	4	3	nd	1	1	1	nd	1	3	1
As	17	18	581	15	17	24	26	30	45	460	17	15	581	114	228	261	525	165	67	67	525	249
Rb	26	6	10	3	14	9	5	9	12	16	6	3	26	11	10	18	34	5	7	5	34	15
Nb	155	156	111	181	155	175	134	163	140	109	154	109	181	148	105	126	110	116	119	105	126	115
Mo	8	5	5	5	6	2	6	3	4	nd	9	2	9	5	4	4	8	6	4	4	6	4
Ag	1.4	1.0	0.5	0.7	1.0	0.7	0.6	nd	0.7	1.3	0.9	0.5	1.4	0.9	1.1	nd	0.6	nd	nd	0.6	1.1	0.8
In	nd	0.3	nd	0.3	0.2	0.4	nd	nd	nd	nd	0.4	0.2	0.4	0.3	nd	nd	nd	nd	nd			
Sn	9	8	6	2	8	8	7	7	7	6	7	6	9	7	5	6	5	nd	6	5	6	5
Sb	2	2	8	2	1	2	2	2	2	6	2	1	8	3	4	4	9	3	3	3	9	4
Cs	1.3	nd	nd	0.7	nd	nd	nd	nd	0.6	0.7	nd	0.6	1.3	0.8	1.0	0.8	2.6	nd	0.5	0.5	2.6	1.2
La	13	26	23	21	8	19	18	128	26	4	23	4	128	28	10	6	52	11	14	6	52	19
Ce	89	173	108	115	209	219	36	288	152	55	183	36	288	148	46	39	157	108	140	39	157	98
Pr	3	6	4	4	2	8	4	24	6	1	6	1	24	6	2	2	8	2	4	2	8	4
Nd	12	21	12	19	8	37	18	84	25	4	22	4	84	24	7	11	21	11	16	7	21	13
Sm	3	5	2	6	2	9	5	15	7	1	6	1	15	6	2	3	5	3	3	2	5	3
Eu	0.9	1.7	0.6	1.9	0.6	2.2	1.4	4.3	1.7	nd	1.6	0.6	4.3	1.7	0.4	1.2	1.0	0.9	1.5	0.4	1.5	1.0
Gd	4	5	2	7	2	8	5	15	7	2	5	2	15	6	2	4	3	3	5	2	5	3
Tb	0.8	0.9	nd	1.3	0.5	1.3	1.0	2.4	1.0	nd	0.8	0.8	2.4	1.2	0.3	0.8	0.6	0.6	0.7	0.3	0.8	0.6
Dy	5	5	2	9	2	7	6	13	5	2	5	2	13	6	2	4	4	3	4	2	4	3
Ho	1.0	1.1	0.5	1.8	0.5	1.4	1.1	2.3	0.9	nd	0.9	0.5	2.3	1.1	0.4	0.8	0.8	0.6	0.7	0.4	0.8	0.7
Er	3	3	3	5	2	4	3	7	nd	nd	3	2	7	3	1	2	2	2	4	1	4	2
Tm	nd	nd	nd	0.8	nd	0.6	nd	1.0	nd	nd	nd	0.6	1.0	0.8	0.2	0.3	0.4	0.3	0.7	0.2	0.7	0.3
Yb	3	3	2	5	2	3	3	6	2	1	3	1	6	3	1	2	2	2	2	1	3	2
Lu	nd	nd	nd	nd	nd	nd	nd	1	nd	nd	nd	1	1	1	0	0	0	0	0	0	1	0
Hf	19	19	13	23	19	22	15	18	16	14	18	13	23	18	12	12	15	13	13	12	15	13
Ta	9	10	7	8	8	8	9	11	9	8	9	7	11	9	7	8	7	7	8	7	8	7
W	22	31	18	64	45	36	16	39	27	13	37	13	64	32	4	12	10	13	15	4	15	11
Tl	0.5	nd	0.2	0.2	0.2	0.1	0.1	0.1	0.1	0.2	nd	0.1	0.5	0.2	0.1	1.2	0.3	0.5	0.9	0.1	1.2	0.6
Pb	20	10	133	21	13	28	10	15	14	22	9	9	133	27	26	23	94	18	18	18	94	36
Bi	2	2	8	9	12	3	7	3	4	3	3	2	22	7	5	6	2	5	7	2	7	5
Th	36	35	25	39	31	34	26	28	26	23	30	23	39	30	22	26	26	19	22	19	26	23
U	22	22	22	29	22	25	16	18	16	12	14	12	29	20	19	11	28	12	8	8	28	16
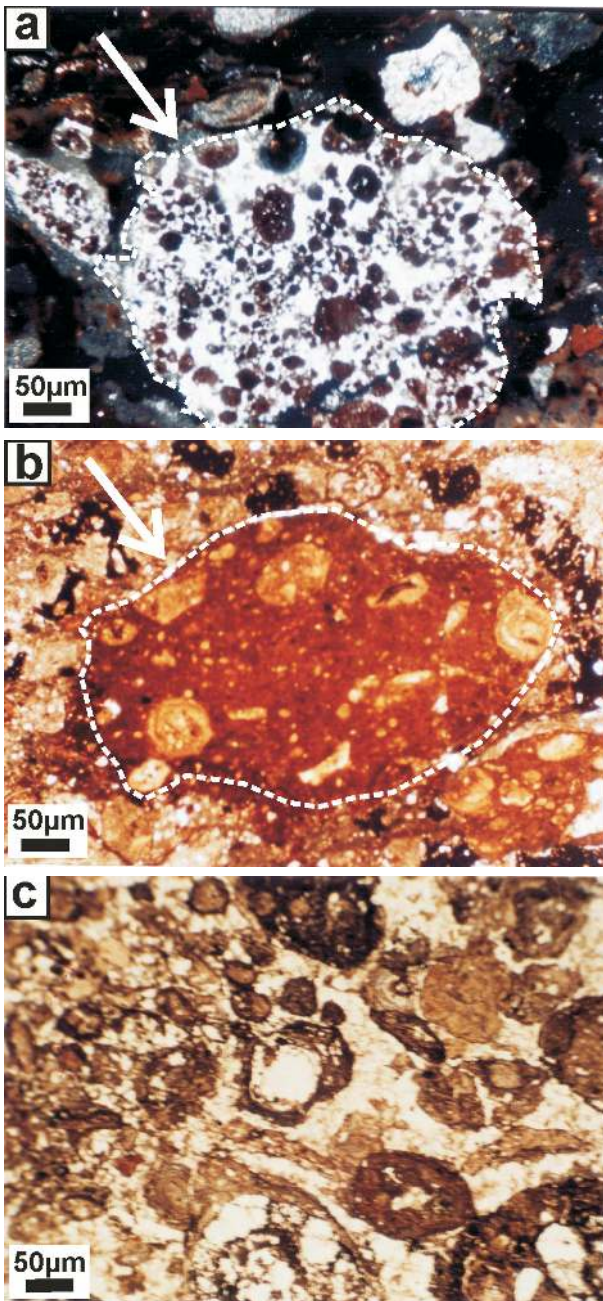
Figure 4. (a) Well-rounded intraclast which is composed of diaspore-cemented intraclasts. It shows several phases of cementation and reworking of bauxitic material, during and after bauxitization (XPL). **(b)** Oolitic texture with reworking features and fine-grained diasporic and iron oxyhydroxides matrix from the red bauxite horizon (PPL). **(c)** Diaspore cemented bauxite with various particle size resulted from alteration, recrystallization and diagenetic processes (PPL).

primary materials were colloidal; large particles formed via secondary processes such as recrystallization and reworking and erosion of complex oolitic clasts (Figure 4a, b). Spherical grains such as ooids and pisoids are important components of most samples (Figure 4b, c). Their presence can be attributed to the heterogeneity of the initial colloids that originated from alteration of the source rock. Another possibility is the formation of these spheroidal particles in terrigenous lateritic weathering crusts. Some pore spaces formed by dissolution in the bauxite samples are filled by minerals such as diaspore, goethite, hematite, and dolomite.

Geochemistry

32 samples were analyzed for major and trace element concentrations, including 11 samples each of bauxitic clay and red bauxite, and 5 samples each of the lower argillaceous layer and the upper kaolinite (Table 1). The dominant chemical components of the samples are Al_2O_3, Fe_2O_3, SiO_2, and H_2O (i.e., loss on ignition (LOI), which was chiefly H_2O, as the samples are free of other volatiles). We found considerable chemical variation both among the four groups of samples and within individual groups (Table 1). In the bauxitic clay and red bauxite, Al_2O_3 contents range between 26.50 and 56.47 wt%, Fe_2O_3 between 2.77 and 34.22 wt%, SiO_2 between 4.31 and 41.75 wt%, and TiO_2 between 2.56 and 7.14 wt%. Relative to the average composition of bauxite deposits (Bronevoi *et al.* 1985), the Jajarm bauxite ore is enriched in the trace elements Ce (36–1080 ppm), Nb (93–180 ppm), Bi (2–22 ppm), and Ta (5.7–10.5 ppm). Relative to crustal averages, the analyzed samples are enriched in Al, Fe, and Ti, and depleted in Mg, Ca, Na, and K. Th concentrations are higher in the red bauxite than in the bauxitic clay, whereas Sc concentrations are similar in the two rock types.

When plotted against Al and Ti, the concentrations of Zr, Nb, and Th produce similarly well-correlated data arrays for samples from all horizons (Figure 5). In addition, most red bauxite samples are enriched in Th, Zr, and Nb. The small degree of variation evident in each plot can be

275
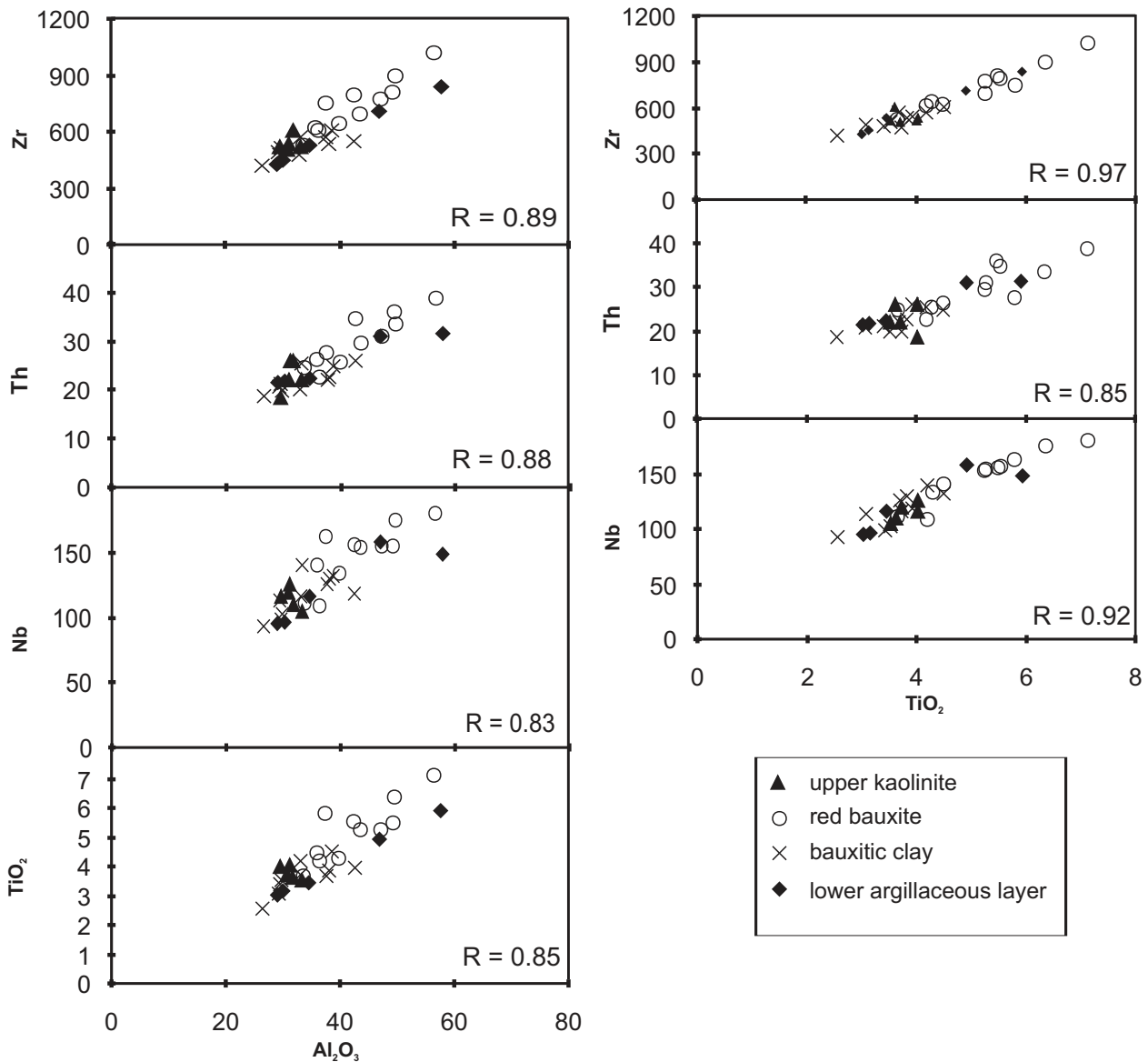
Figure 5. Binary plots of some immobile trace elements (ppm) against Al_2O_3 and TiO_2 (wt%).

attributed to minor element mobility, weak source-rock heterogeneity, or the local winnowing of lateritized minerals during subaerial weathering. The latter process tends to separate heavy minerals containing elements such as Ti, Zr, and Nb from the lighter Al-bearing kaolinite and diaspore.

The average rare earth element (REE) concentrations vary from 0.5 ppm for Lu and Tm in red bauxite up to 225 ppm for Ce in bauxitic clay (Tables 1 & 2). These elements, especially the light

REE (LREE), are concentrated in the bauxitic clay rather than the red bauxite. The chondrite-normalized REE patterns obtained for the upper kaolinite layer are similar to those for the underlying red bauxite, while the patterns obtained for the lower argillaceous layer are similar to those for the overlying bauxitic clay (Figure 6).

Puchelt & Emmerman (1976) explained a strong connection between REE ionic potential and their mobility. This is consistent with the distribution
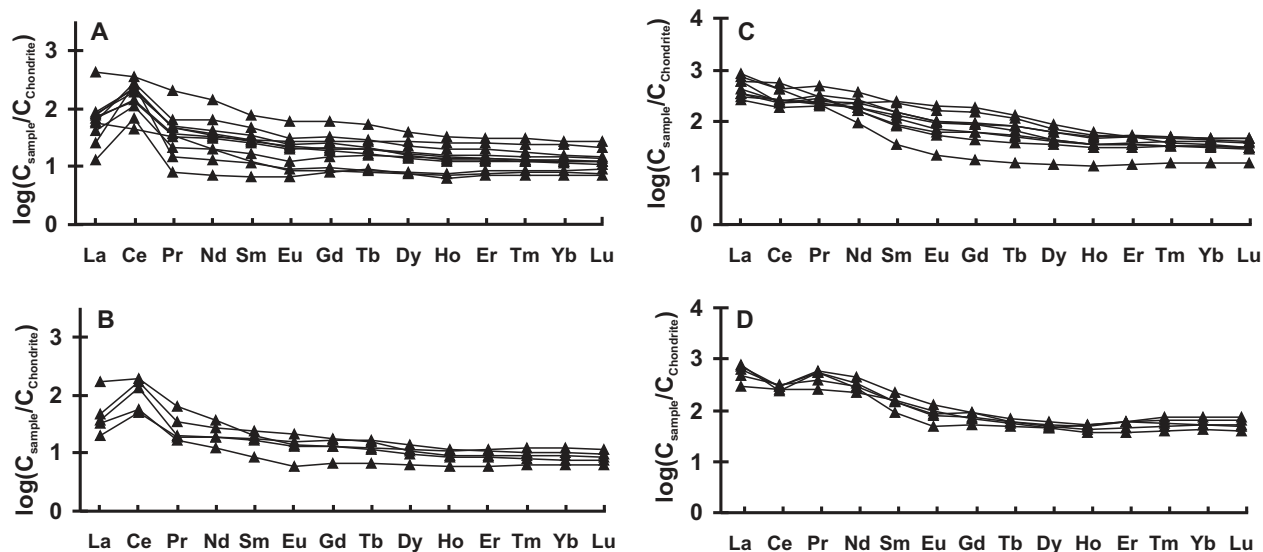
Figure 6. Chondrite normalized REE patterns of **(A)** red bauxite, **(B)** upper kaolinite, **(C)** bauxitic clay and **(D)** lower argillaceous layer.

pattern of REE in the Jajarm bauxite deposit. Ce shows a positive anomaly in the red bauxite and upper kaolinite layer and a weak negative anomaly in the lower argillaceous clay layer. Ce exists naturally in two forms: Ce^{3+} and Ce^{4+}, with the latter having a higher ionic potential than the other LREE and consequently the lowest mobility. Accordingly, the positive Ce anomaly observed in the red bauxite can be explained by its occurrence as Ce^{4+} ions. The lower ionic potential of LREE relative to HREE means that they were readily leached from the red bauxite and concentrated in the bauxitic clay (Tables 1 & 2). In contrast, the high ionic potential of Ce^{4+} means that it behaved as a HREE, and was concentrated in the bauxitic clay.

Although the ionic potential of HREE increases from Er to Lu, this trend does not appear to affect their concentrations in the bauxitic clay. A relatively high correlation coefficient among Er, Tm, Yb, Lu (HREE) and Zr and Al in the red bauxite (Table 2) may indicate that the HREE are more commonly accompanied by minerals containing Zr and Al (mostly clay minerals and zircon). Therefore, in addition to the ionic potential of the REE, their host-mineral chemistry may also have been an important factor in determining their degree of leaching. The strong correlations between REE (except La), Nb, and TiO_2 (Table 2), suggest these REE are probably hosted by oxides of Ti and Nb (e.g., Gonzáles López *et al.* 2005). High correlation coefficients obtained

Table 2. Average concentrations of REE in red bauxite and bauxitic clay samples from the study area.

	TiO_2	Al_2O_3	Zr	Cr	Sn	Nb	La	Ce	Pr	Nd	Sm	Eu	Gd	Tb	Dy	Ho	Er	Tm	Yb	Lu	REE
TiO_2	1.00					0.99	0.26	0.58	0.51	0.50	0.64	0.77	0.71	0.68	0.77	0.79	0.79	0.80	0.80	0.78	0.60
Al_2O_3		1.00					-0.26	0.25	0.00	0.05	0.20	0.34	0.31	0.28	0.42	0.46	0.46	0.51	0.51	0.49	
Zr			1.00				-0.01	0.37	0.24	0.24	0.39	0.55	0.50	0.46	0.61	0.65	0.65	0.67	0.67	0.64	
Cr				1.00			-0.17	0.21	0.03	0.03	0.15	0.28	0.25	0.16	0.34	0.43	0.43	0.46	0.46	0.44	
Sn					1.00		-0.07	0.32	0.12	0.13	0.28	0.42	0.37	0.30	0.46	0.54	0.54	0.56	0.56	0.53	
Nb						1.00	0.32	0.60	0.55	0.53	0.65	0.78	0.72	0.66	0.76	0.80	0.80	0.81	0.81	0.79	

for Ti–Nb (0.99) and Ti–ΣREE (0.6) demonstrate that Nb- and Ti-bearing minerals such as anatase determined the distribution of some of the REE. Other titanium and niobium oxides such as loparite and euxenite (Mariano 1989) may also have influenced the distribution of some of the REE in these rocks, as REE and Y can be replaced by Ca in the mineral structure.

Discussion and Conclusion

Diagenetic and Epigenetic Processes

Different diagenetic processes in the Jajarm bauxite deposit formed ooids and pisoids, as well as the replacement of boehmite by diaspore. Also, these spheroidal particles could have been formed by terrigenous lateritic weathering crusts. Like many other diasporic deposits (Nikitina 1986; Bárdossy & Aleva 1990) the original mineralogical composition of the Jajarm bauxite appears to have been gibbsitic, which altered to boehmite then to diaspore during diagenesis.

Epigenetic processes that began after dehydration and crystallization of the primary gel were enhanced by burial or tectonic pressures, resulting in chemical and physical deformation (e.g., pressure solution and stylolites; Figure 7a). These burial pressures may well have led to alteration of boehmite to diaspore. The textures observed in the Jajarm bauxite indicate that the initiation of bauxite formation occurred under reducing conditions, followed later by oxidizing conditions (hematite formation). Accordingly, local reducing conditions were dominated by the deposition of the OM-rich Shemshak formation on
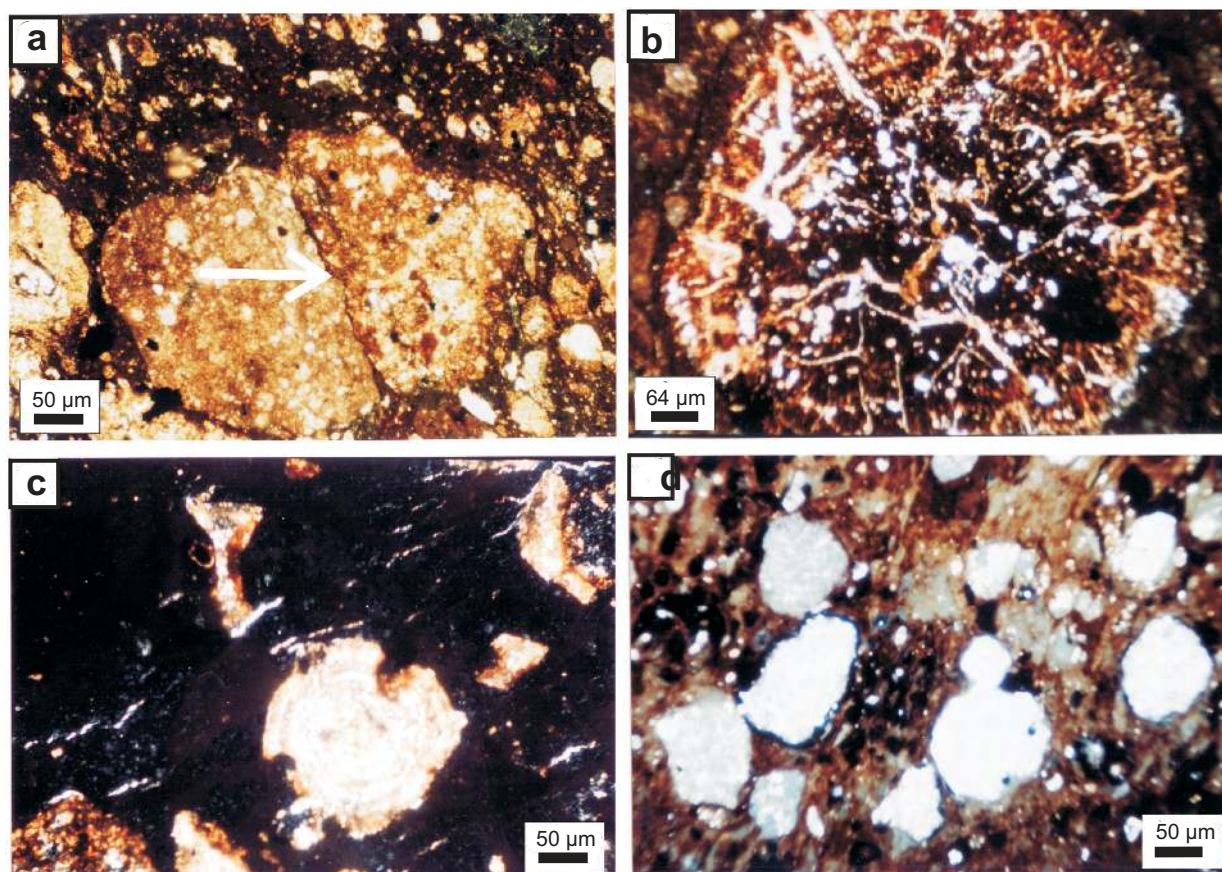
Figure 7. (a) Pressure-solution fabric in the reworked diasporic clasts, formed during burial (XPL). **(b)** Grain-bounded epigenetic fractures in a pisolite grain from red bauxite horizon (XPL). **(c)** Epigenetic micro-fractures that cross-cut the matrix of red bauxite sample (XPL). **(d)** An intraclast in a fine-grained matrix formed by deferrification.

the bauxitic horizons. This coal-rich formation was deposited in a series of paralic marshes covering the bauxitic horizon. Then, due to oxidation of organic matter, Fe was stabilized as soluble ferrous ions (Biber *et al.* 1994).

As mentioned, leaching of mobile elements from the upper horizon (red bauxite) and deposition within the lower (bauxitic clay) is another epigenetic process (e.g., Valeton *et al.* 1987). Another important epigenetic process was deferrification, and the leaching of iron, which occurs at all scales from the macro to the micro; with the conversion of hematite into limonite, is one of the results of this process. Deferrification provides evidence of microbial and biological activity that produced acidic and reducing conditions (Augustithis 1982). Generally, biological and herbal activities decrease the pH of sedimentary environments: this reduces Fe^{3+} to Fe^{2+} and finally causes iron to be leached from iron-bearing minerals as organometallic complexes. In the Jajarm bauxite the degree of deferrification is variable and traceable either in different layers of a single ooid and pisoid or in different beds with variable amounts of deferrification (Figure 7d).

Fractures and joints are the other important epigenetic features of the deposit, and these are divided into two main groups. The first group is confined to within individual grains (e.g., within pisoids), terminating at grain boundaries (Figure 7b). These fractures originated from the dehydration and compaction of the original material. The second group of fractures cuts through the matrix, and individual fractures are of varying origin. Some formed following the dehydration of the original bauxite-forming material, while others are of tectonic origin and transect both grains and the surrounding matrix (Figure 7c). Various fractures, joints, and veinlets are filled with materials such as diasporic and boehmitic cement that in some samples occur as coarse crystals; other infill minerals are hematite, goethite, pyrite, Mn oxides, ankerite, etc.

Source Rock Material

Many bauxite deposits can be directly related, via texture and chemistry, to the underlying bedrock;

although in sedimentary limestone sequences we are faced with a wider array of choices, ranging from argillite components of the underlying limestone to fluvially transported debris sourced from basement rocks (e.g., Bárdossy 1982, 1984) and deposits of volcanic ash (Bárdossy 1984; Lyew-Ayee 1986). In all these models, Al is concentrated *in situ* as an inert (immobile) residue of lateritization.

In studies of other deposits, Pye (1988) and Brimhall *et al.* (1988) proposed windborne transport as the re-concentration process that formed local high-grade bauxites. Given the nature of karst erosion, in which both chemical and mechanical weathering is active, it is generally difficult to determine the relative contributions of different sources of argillaceous debris during bauxite formation.

The concentrations of immobile elements can be used to trace source materials, as they show contrasting distributions in different sources. In this study, variation diagrams for Zr, Nb, and Th versus Al_2O_3 and TiO_2 (Figure 5) demonstrate a single strongly correlated trend for all four main horizons within the bauxite deposit. Based on the findings of MacLean (1990), the four horizons within the Jajarm bauxite appear to have originated from a single homogeneous source. In the Ni-Cr diagram (Figure 8), the Jajarm bauxite samples plot close to the karstic bauxite field with a basaltic source material (see Schroll & Sauer 1968). According to the Zr-Cr (Ni)-Ga ternary diagram of Balasubramaniam *et al.* (1987), our samples generally show a mixed origin of basic igneous and sedimentary rocks (Figure 9).

In considering the concentrations or proportion of selected trace elements, Mordberg (1993) proposed several variation diagrams that can be used to distinguish the mineralogical composition of bauxite deposits of different ages. Contrary to the diasporic mineralogical composition of the Jajarm bauxite, Mordberg's plot indicates an original gibbsitic mineralogical composition (Figure 10). This observation suggests that an original gibbsitic composition converted to diaspore over time.

REE patterns can also be used to identify source materials (e.g., González López *et al.* 2005). Chondrite-normalized REE patterns obtained for the Jajarm bauxite resemble those of the composition of upper continental crust (UCC) (Figure 11) and shale
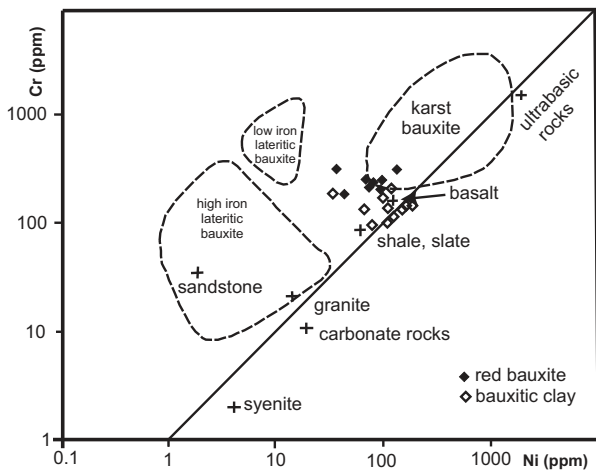
Figure 8. Binary correlation diagram of Cr/Ni in karst and lateritic bauxites in different parent rocks (after Schroll & Sauer 1968).
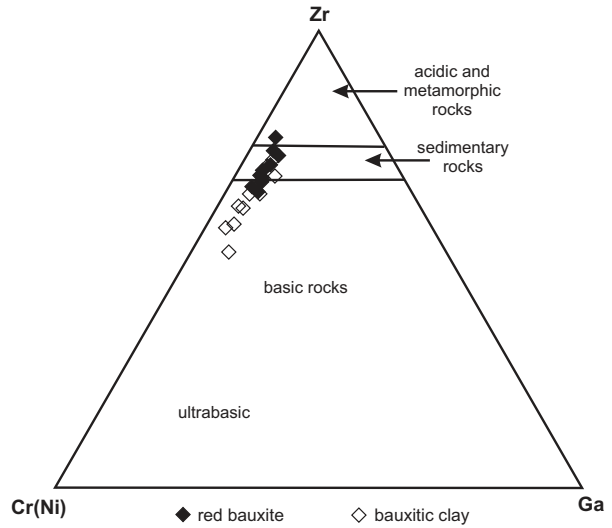

Figure 9. Zr-Cr(Ni)-Ga ternary diagram for bauxites derived from different parent rocks (Balasubramaniam *et al.* 1987).
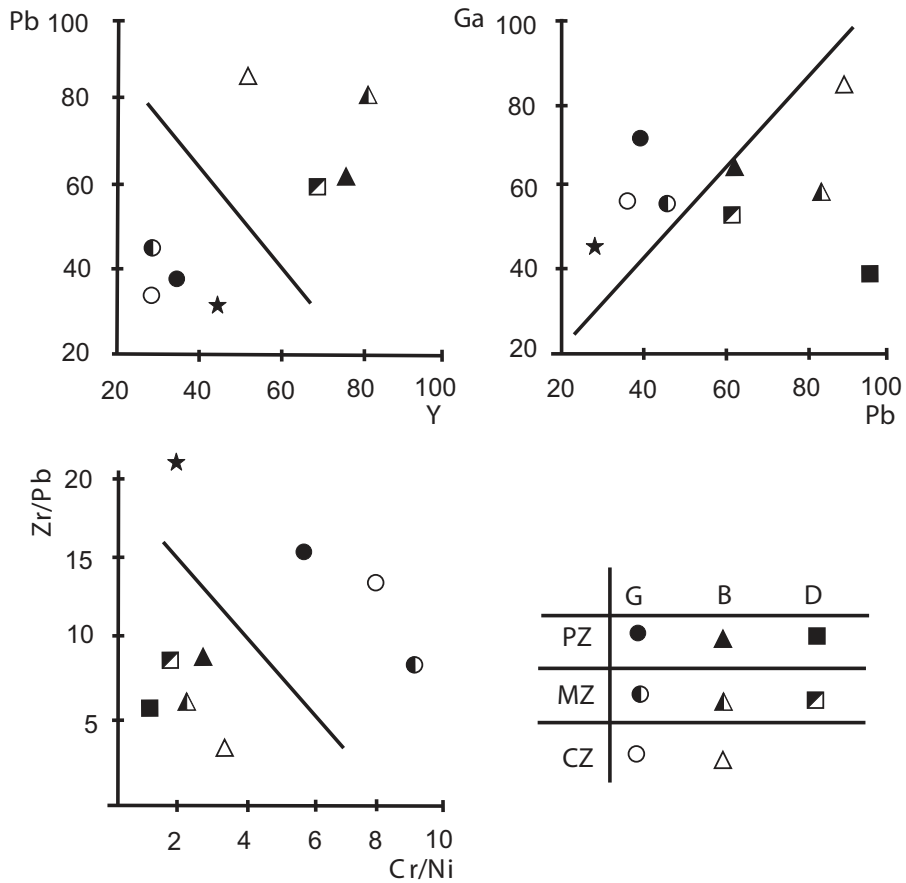

Figure 10. Trace element ratios in bauxites of different ages and mineral forms of Al (G– gibbsite; B– boehmite; D– diaspore; PZ– Palaeozoic; MZ– Mesozoic; CZ– Cenozoic) (Mordberg 1993). Jajarm bauxite samples are shown by stars.

(Figure 12). HREE patterns for the Jajarm bauxite are closely related to those for diabase, although with some enrichment (Figures 11 & 12). The fact that REE patterns obtained for the bauxite are similar to those for UCC and shale can be explained by the mixed origin of the source material: bauxitization was initiated on the basic source rock, but continued during reworking and replacement within the karstic features. A contribution from sedimentary material during the latter process explains the observed REE patterns.

The palaeogeography of Iran in the Late Permian and Early Triassic indicates that the early Late Triassic compressional phase (Early Cimmerian Event) was followed by extensional movements in North and Central Iran. The initiation of this extensional phase is locally indicated by continental alkali-rift basaltic lava flows and vesicular mafic rocks (ranging from a few metres up to 300 m thick) (Berberian & King 1981; Vollmer 1987). In the Alborz mountains (Figure 1), the Late Triassic andesitic to basaltic volcanic rocks cover an eroded and often karstified surface of Middle Triassic carbonates (Early Cimmerian palaeorelief), at the base of the Shemshak formation (for example Firoozkouh and Shahmirzad in Figure 1) (Annelles *et al.* 1975; Nabavi & Seyed-Emami 1977; Nabavi 1987). The volcanic activity occasionally continued into the lower part of the Shemshak formation. So the proposed basic source material of the Jajarm bauxite is widespread within the Elika formation in certain parts of Alborz Mountain Range. This interpretation of a basic source material is supported by petrographic evidence, such as the replacement of igneous feldspar by platy diaspore and the well-rounded nature of reworked oolitic and pisolitic grains.

Origin of Bauxite Layering

Geochemical results (Table 1) demonstrate the enrichment of less mobile elements (such as Nb, Th, Zr, Mo, Ga, and Cr) and the depletion of mobile elements (such as Rb, K, Na, Sr, La, Mg, and Pb) in the red bauxite relative to the bauxitic clay. This
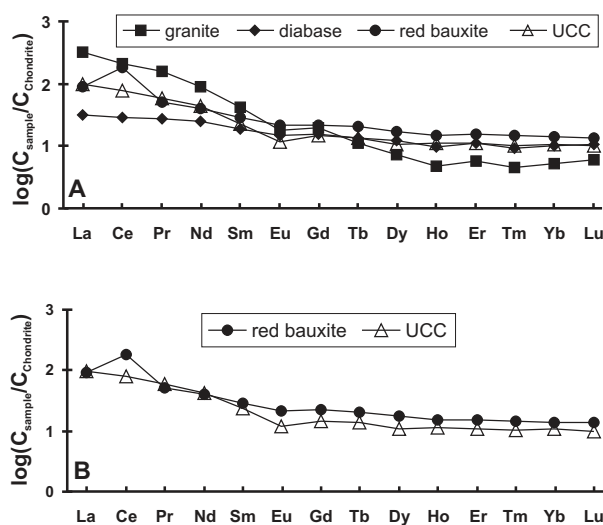
Figure 11. Comparison of chondrite normalized patterns of red bauxite and Upper Continental Crust (UCC) (Taylor & McLennan 1981), as well as granitic and diabasic rocks (Klein & Hurlbut 1999). The chondritic composition is after Boynton (1984). Diagram A is for comparison of chondrite normalized patterns of red bauxite with granitic, diabasic and UCC composition. The red bauxite and UCC are compared in diagram B.
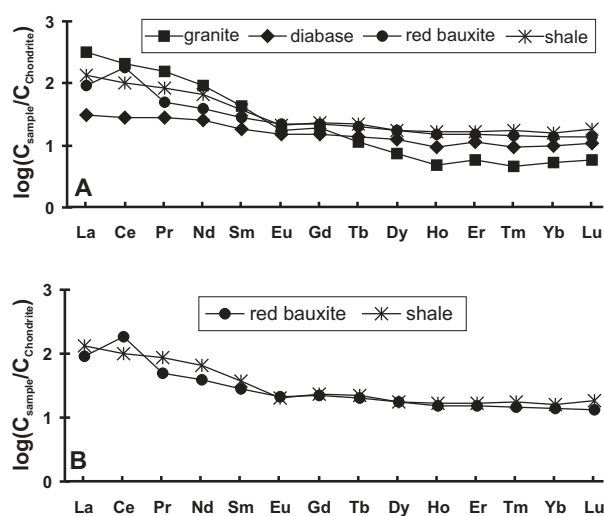
Figure 12. Comparison of chondrite normalized patterns of red bauxite with average composition of European shale (Haskin & Haskin 1966), granitic and diabasic rocks (Klein & Hurlbut 1999). The chondritic composition is after Boynton (1984). Diagram A is for comparison of chondrite normalized patterns of red bauxite with granitic, diabasic and average composition of European shales. The red bauxite and European shale are compared in diagram B.

281

pattern could reflect the leaching of mobile elements from the upper horizon (red bauxite) and deposition within the lower (bauxitic clay). Such a trend is also described from other karst-hosted bauxite deposits (e.g., Valeton *et al.* 1987; Maksimović & Pantó 1991; MacLean *et al.* 1997). In addition, the carbonate host acted as a geochemical barrier to further migration of the mobilized elements, leading to their concentration in the lowermost horizon. A lack of active drainage in the bauxitic clay and the nature of its interface with carbonate rocks are the main reasons for the dominance of basic pH values. This explains the weak bauxitization observed in the lower horizon and the evolution of the bauxitic clay. In comparison, the occurrence of active drainage and acidic pH in the red bauxite acted to enhance the bauxitization process.

Chondrite-normalized REE values are similar for both the bauxitic clay and the lower argillaceous horizon, while the values for the red bauxite are similar to those for the upper kaolinite horizon (Figure 6). These findings indicate a similar origin for the lower argillaceous horizon and the bauxitic clay on one hand, and a similar origin for the upper kaolinite horizon and red bauxite on the other. The direct interface of the lower argillaceous layer with the carbonate footwall, and relatively poor drainage condition in the lowermost part of the deposit caused separation of the bauxitic clay and the lower argillaceous layer as both have different mineralogical and geochemical properties.

In contrast to the lower argillaceous horizon, the upper kaolinite horizon is relatively homogeneous in terms of chemical and mineralogical composition, with kaolinite being the most abundant mineral. The upper 1–4 m of the red bauxite is completely replaced by secondary kaolinite, and the lower boundary of this horizon with the red bauxite is irregular but sharp. Resilification could be the origin of the Si for secondary kaolinite. According to Bárdossy & Aleva (1990, p. 181–182) in some deposits, secondary kaolinite completely replaces the upper part of the bauxite horizon and dissolved silica is introduced into the bauxite horizon by the ground water, either laterally or from the overburden. The optimum pH for kaolinitization is close to 4 (Yariv & Cross 1979, p. 321–324), and it generally involves a high degree of crystallization (Bárdossy & Aleva 1990). This high acidity resulted from the development of swamps upon the red bauxite during Early Jurassic deposition of the Shemshak formation (Figure 2). Dominance of swamps and reducing conditions is evident from the presence of the overlying Shemshak formation (in a large area in north and central of Iran), containing a huge amount of organic materials such as coal and kerogen, formed mainly in a deltaic environment.

Acknowledgments

References

ANNELLES, R.N., ARTHURTON, R.S., BAZELY, R.A. & DAVIES, R.G. 1975. *E3-E4 Quadrangle, 1:100 000 Scale Geological Map and Explanatory Text of Qazvin and Rasht.* Geological Survey of Iran, Tehran.

AUGUSTITHIS, S.S. 1982. *Atlas of the Sphaeroidal Textures and Structures and their Genetic Significance.* Theophrastus S.A. Athens.

BALASUBRAMANIAM, K.S., SURENDRA, M. & RAVIKUMAR, T.V. 1987. Genesis of certain bauxite profiles from India. *Chemical Geology* **60**, 227–235.

BÁRDOSSY, G. 1982. *Karst Bauxite.* Development in Economic Geology **14**, Elsevier, Amsterdam.

BÁRDOSSY, G. 1984. European bauxite deposits. *In*: JACOB, L.JR. (ed), *Proceedings of International Bauxite Symposium.* Society of Mining Engineers, New York, 411–435.

BÁRDOSSY, G. & ALEVA, J.Y.Y. 1990. *Lateritic Bauxites.* Developments in Economic Geology **27**, Elsevier, Amsterdam.

BERBERIAN, F. & BERBERIAN, M. 1981. Tectono-plutonic episodes in Iran. *In*: GUPTA, H.K. & DELANY, F.M. (eds), *Zagros, Hindu Kush, Himalaya Geodynamic Evolution.* American Geophysical Union Geodynamics Series **3**, 5–32.

BERBERIAN, M. 1983. *Continental Deformation in the Iranian Plateau.* Geological Survey of Iran, report **52**.

BERBERIAN, M. & KING, G.C.P. 1981. Towards a paleogeography and tectonic evolution of Iran. *Canadian Journal of Earth Sciences* **18**, 210–265.

BIBER, M.V., DOS SANTOS, A. & STUMM, W. 1994. The coordination chemistry of weathering: IV. inhibition of the dissolution of oxide minerals. *Geochimica et Cosmochica Acta* **58**, 1999–2010.

BOYNTON, W.V. 1984. Cosmochemistry of the rare earth elements: meteorite studies. *In*: HENDERSON, P. (ed), *Rare Earth Element Geochemistry.* Elsevier, 63–114.

BRIMHALL, G.H., LEWIS, C.J., AGUE, J.J., DIETRICH, W.E., HAMPEL, J. & RIX, P. 1988. Metal enrichment in bauxites by deposition of chemically mature aeolian dust. *Nature* **333**, 819–824.

BRINDLEY, G.W. 1981. Structures and chemical compositions of clay minerals. *In*: LONGSTAFFE, F.J. (ed), *Clays and the Resource Geologist Calgary.* Mineralogical Association of Canada, 1–21.

BRONEVOI, V.A., ZHILBERMINC, A.V. & TEENIAKOV, V.A. 1985. Average chemical composition of bauxites and their evolution in time. *Geokhimia, Moscow* **4**, 435–446 [in Russian].

BRÖNNIMANN, P., ZANINETTI, L., MOSHTAGHIAN. A. & HUBER, H. 1973. Foraminifera from the Sorkh Shale formation of the Tabas area, East-Central Iran. *Rivista Italiana Dipaleontologia e Stratigrafia* **79**, 1–32.

COTTEN, J., LE DEZ, A., BAU, M., CAROFF, M., MAURY, R.C., DULSKI, P., FOURCADE, S., BOHN, M. & BROUSSE, R. 1995. Origin of anomalous rare-earth element and yttrium enrichment in subaerially exposed basalts: evidence from French Polynesia. *Chemical Geology* **119**, 115–138.

DEDECKER, D. & STOOPS, G. 1999. A morpho-synthetic system for the higher level description of microfabrics of bauxitic and kaolinitic soils. A first approximation. *Catena* **35**, 317–326.

ELIOPOULOS, D.G. & ECONOMOU-ELIOPOULOS, M. 2000. Geochemical and ineralogical characteristics of Fe-Ni- and bauxitic-laterite deposits of Greece. *Ore Geology Reviews* **16**, 41–58.

FURIAN, S. 1994. *Morphogenèserpédogenèse en milieu tropical humide de la Serra do Mar, Bresil: Contribution de l'altération et de la pédogenèse á une dynamique actuelle de glissement.* PhD Thesis, Université de Caen, France [unpublished].

GONZÁLEZ-LÓPEZ, J.M., BAULUZ, B., FERNÁNDEZ-NIETO, C. & OLITE A.Y. 2005. Factors controlling the trace-element distribution in fine-grained rocks: the Albian kaolinite-rich deposits of the Oliete Basin (NE Spain). *Chemical Geology* **214**, 1–19.

GRUBB, P.L.C. 1963. Critical factors in the genesis, extent and grade of some residual bauxite deposits. *Economic Geology* **58**, 1267–1277.

HASKIN, M.A. & HASKIN, L.A. 1966. Rare earths in European shales: a redetermination. *Science* **154**, 507–509.

HOOPER, R.J., BARON, I., HATCHER JR., R.D. & AGAH, S. 1994. The development of the southern Tethyan margin in Iran after the break up of Gondwana: implications of the Zagros hydrocarbon province. *Geosciences* **4**, 72–85.

IIJIMA, A. & MATSUMOTO, R. 1982. Berthierine and chamosite in coal measures of Japan. *Clays and Clay Minerals* **30**, 264–274.

KLEIN, C. & HURLBUT, C.S.Jr. 1999. *Manual of Mineralogy.* Revised 21th Edition. John Wiley and Sons. INC, 315–320.

LYEW-AYEE, P.A. 1986. A case for the volcanic origin of Jamaican bauxites. *Journal of the Geological Society of Jamaica*, 9–39.

MACLEAN, W.H., BONAVIA, F.F. & SANNA. G. 1997. Argillite debris converted to bauxite during karst weathering: evidence from immobile element geochemistry at the Olmedo deposit, Sardinia. *Mineralium Deposita* **32**, 607–616.

MACLEAN, W.H. 1990. Mass change calculations in altered rock series. *Mineralium Deposita* **25**, 44–49.

MAKSIMOVIĆ, Z. & PANTÓ, G. 1991. Contribution to the geochemistry of the rare earth elements in the karst-bauxite deposits of Yugoslavia and Greece. *Geoderma* **51**, 93–109.

MARCOUX, J. 1993. Late Permian to Triassic Tethyan paleoenvironments. *Conference on Carboniferous to Jurassic of PANGEA,* Abstract with Program, 15–17.

MARIANO, A.N. 1989. Economic geology of rare earth minerals. *In*: LIPIN, B.R. & MCKAY, G.A. (eds), *Geochemistry and Mineralogy of Rare Earth Elements.* Mineralogical Society of America, Reviews in Mineralogy **21**, 309–336.

MORDBERG, L.E. 1993. Patterns of distribution and behaviour of trace elements in bauxites. *Chemical Geology* **107**, 241–244.

MORDBERG, L.E. 1999. Geochemical evolution of a Devonian diaspore-crandallite–svanbergite-bearing weathering profile in the Middle Timan, Russia. *Journal of Geochemical Exploration* **66**, 353–361.

MUTAKYAHWA, M.K.D., IKINGURA, J.R. & MRUMA, A.H. 2003. Geology and geochemistry of bauxite deposits in Lushoto District, Usambara Mountains, Tanzania. *Journal of African Earth Sciences* **36**, 357–369.

NABAVI, M. H. 1987. *Geological Map of Semnan Sheet, 1:100,00 Scale.* Geological Survey of Iran, Tehran.

NABAVI, M. H. & SEYED-EMAMI, K. 1977. Sinemudan ammonites from the Shemshak formation of North Iran (Semnan area, Alborz). *Neues Jahrbuch fur Geologie und Palaontologie-Abhandlungen* **153**, 70–85.

NAHON, D.B. 1991. *Introduction to the Petrology of Soils and Chemical Weathering.* Wiley, New York.

NIKITINA, A.P. 1986. Types of residual bauxites of the KMA area, conditions of their formation and preservation. *Kora Vyvetrivania (Weathering Crust), Moscow* **19**, 106–116 [in Russian].

ÖZTÜRK, H., HEIN, J.R., HANILCI, N. 2002. Genesis of the Doğankuzu and Mortaş bauxite deposits, Taurides, Turkey: separation of Al, Fe, and Mn and implications for passive margin metallogeny. *Economic Geology* **97**, 1063–1077.

PRICE, G.D., VALDES, P.J. & SELLWOOD, B.W. 1997. Prediction of modern bauxite occurrence: implications for climate reconstruction. *Palaeogeography, Palaeoclimatology, Palaeoecology* **131**, 1–13.

PUCHELT, H. & EMMERMANN, R. 1976. Bearing of rare earth patterns of appetites from igneous and metamorphic rocks. *Earth and Planetary Science Letters* **31**, 279–286.

PYE, K. 1988. Bauxites gathering dust. *Nature* **333**, 800–801.

SCHROLL, E. & SAUER, D. 1968. Beitrag zur Geochemie von Titan, Chrom, Nickel, Cobalt, Vanadium und Molibdän in bauxitischen Gesteinen und das Problem der stofflichen Herkunft des Aluminiums. *Travaux de l'ICSOBA, Zagreb* **5**, 83–96.

SEYED-EMAMI, K., FÜRSICH, F.T., WILMSEN, M., SCHAIRER, G. & MAJIDIFARD, M.R. 2005. Toarcian and Aalenian (Jurassic) ammonites from the Shemshak formation of the Jajarm area (eastern Alborz, Iran). *Palaontologische Zeitschrift* **79**, 349–369.

SHAFFER, J.W. 1975. Bauxite raw materials. *In*: *Industrial Minerals and Rocks (Non-metallic other than Fuels)*. American Institute of Mining and Metallurgical, and Petroleum Engineering, 442–459.

STAMPFLI, G., ZANINETTI, L., BRÖNIMANN, P., JENNY-DESHUSSES, C. & STAMPFLI-VUILLE, B. 1976. Trias de I'Elburz oriental, Iran. Stratigraphie, sédimentologie, micropaléontologie. *Rivista Italiana di Paleontologia e Stratigrafia* **82**, 467–500.

STÖCKLIN, J., EFTEKHAR-NEZHAD, J. & HUSHMAND-ZADEH, A. 1965. *Geology of the Shotori Range (Tabas area, East lran)*. Geological Survey of Iran, Tehran, report **3**.

TAYLOR, S.R. & McLENNAN, S.M. 1981. The composition and evolution of the continental crust: rare earth element evidence from sedimentary rocks. *Philosophical Transactions of the Royal Society of London Series A* **301**, 381–399.

VALETON, I., BIERMANN, M., RECHE, R., ROSENBERG, F. 1987. Genesis of nickel laterites and bauxites in Greece during the Jurassic and Cretaceous, and their relation to ultrabasic parent rocks. *Ore Geology Reviews* **2**, 359–404.

VELDE, B. 1992. *Introduction to Clay Minerals: Chemistry, Origins, Uses and Environmental Significance*. Chapman & Hall, London.

VOLLMER, T. 1987. Zur Geologie des nördlichen Zentral-Elburz zwischen Chalus- und Haraz-Tal, Iran. *Mitteilungen des Geologisch-Paläontologischen Instituts der Universitat of Hamburg* **63**, 1–125.

YARIV, S. & CROSS, H. 1979. *Geochemistry of Colloid Systems*. Springer Verlag, Berlin.